HHS Public Access

Author manuscript

Sci Signal. Author manuscript; available in PMC 2022 December 10.

Published in final edited form as:

Sci Signal. 2022 October 04; 15(754): eabj4009. doi:10.1126/scisignal.abj4009.

The kinase PLK1 promotes the development of *Kras*/*Tp53*-mutant lung adenocarcinoma through transcriptional activation of the receptor RET

Yifan Kong[1,2], **Derek B. Allison**[2,3], **Qiongsi Zhang**[1,2], **Daheng He**[2], **Yuntong Li**[2], **Fengyi Mao**[1,2], **Chaohao Li**[1,2], **Zhiguo Li**[1,2], **Yanquan Zhang**[1,2], **Jianlin Wang**[1,2], **Chi Wang**[2], **Christine F. Brainson**[1,2], **Xiaoqi Liu**[1,2,*]

[1]Department of Toxicology and Cancer Biology, University of Kentucky, Lexington, Kentucky, 40536, USA

[2]Markey Cancer Center, University of Kentucky, Lexington, Kentucky 40536, USA

[3]Department of Pathology and Laboratory Medicine, University of Kentucky, Lexington, Kentucky 40536, USA

Abstract

Increased abundance of polo-like kinase 1 (PLK1) is observed in various tumor types, particularly in lung adenocarcinoma (LUAD). Here, we found that PLK1 accelerated the progression of LUAD through a mechanism that was independent of its role in mediating mitotic cell division. Analysis of human tumor databases revealed that increased PLK1 abundance in LUAD correlated with mutations in KRAS and p53, with tumor stage, and with reduced survival in patients. In a mouse model of $KRAS^{G12D}$-driven, p53-deficient LUAD, PLK1 overexpression increased tumor burden, decreased tumor cell differentiation, and reduced animal survival. PLK1 overexpression in cultured cells and mice indirectly increased the expression of the gene encoding the receptor tyrosine kinase RET by phosphorylating the transcription factor TTF-1. Signaling by RET and mutant KRAS in these tumors converged to activate the mitogen-activated protein kinase (MAPK) pathway. Pharmacological inhibition of the MAPK-pathway kinase MEK combined with inhibition of either RET or PLK1 markedly suppressed tumor growth. Our findings show that PLK1 can amplify MAPK signaling and reveal a potential target for stemming progression in lung cancers with high PLK1 abundance.

*Corresponding author. Xiaoqi.Liu@uky.edu.

Author contributions: Conceptualization: XL, YK, ZL, YZ. Methodology: YK, CFB, QZ, DH, YL, CW, FM, CL, XL. Investigation: YK, DBA, QZ, DH, YL, FM, CL, XL. Visualization: YK, DBA, QZ, YZ, ZL, XL. Funding acquisition: XL, YK. Project administration: XL, YK. Supervision: DBA, CW, CFB, XL. Writing – original draft: YK, DBA. Writing – review & editing: DBA, CFB, XL.

Conflict of interests: The authors declare no potential conflicts of interest.

SUPPLEMENTARY MATERIALS
Figs. S1 to S8
Table S1
Data file S1

INTRODUCTION

Lung cancer is the leading cause of cancer-related death in the United States, with 236,740 new cases and 130,180 deaths estimated in 2022 (1). Non-small-cell lung cancer (NSCLC) is the major subclassification, accounting for more than 80% of all lung malignancies (2). Histologically, NSCLC can be divided into several subtypes: large cell carcinoma, adenocarcinoma, squamous cell carcinoma, and mixed histology tumors (3). Among these subtypes, lung adenocarcinoma (LUAD) is most common, constituting 40%–50% of all NSCLC cases (4). Various molecular targets through overexpression, dysregulation, or oncogenic driver mutations have been identified in NSCLC; these include the genes *EGFR*, *ALK*, *KRAS*, *HER2*, and *RET* (5). In cases of LUAD, the most prevalent oncogenic mutations are gain-of-function mutations in *KRAS* and loss-of-function mutations in p53, which are present in ~30% and ~70% of cases, respectively (6). In the past decade, substantial advancements have been achieved in developing targeted therapies for distinct subtypes of NSCLC, but treatment options for the patients with KRAS-mutant subtypes are unsatisfactory (7). With the exception of $KRAS^{G12C}$ (8–10), KRAS mutants lack a successful, direct inhibitor (11). Instead, most strategies targeting KRAS-mutant tumors focus on its downstream effectors, yet these still yield only limited success (12). Therefore, a greater understanding of the pathogenesis of KRAS-mutant LUAD could lead to new, potentially more effective therapeutic approaches.

Polo-like kinase 1 (PLK1), a serine/threonine protein kinase, is well known for its roles in regulation of cell division in eukaryotic cells. Established roles of PLK1 include the regulation of mitotic entry (13), spindle assembly (14), kinetochore function (15), centrosome maturation (16), cytokinesis (17), and APC/C activity (18). In addition, PLK1 plays critical roles in multiple non-mitotic events, such as DNA replication, p53 regulation, and chromosome dynamics (19). Because of its involvement in both mitotic and non-mitotic processes, PLK1 has received much interest in basic and clinical studies. PLK1 is overexpressed in a broad spectrum of human cancers (20). In the case of NSCLC, PLK1 expression is greater in NSCLC cell lines and tumors compared to normal human bronchial epithelial cell lines and non-tumor tissues, and its overexpression is correlated with unfavorable patient outcomes (21, 22). Also, small-molecule inhibitors targeting PLK1 have been widely studied in cell culture experiments and in clinical trials for NSCLC; however, only modest efficacy was observed in NSCLC patients through phase II trials (23). Here, we used the $Kras^{G12D}$ and $Tp53^{fl/fl}$ (KP)-driven LUAD murine model, which recapitulates many key aspects of human LUAD, to study whether and how PLK1 affects the progress of the disease and uncovered a transcriptional mechanism through which PLK1 enhances the activity of a KRAS-driven signaling pathway. Our findings reveal potential new therapeutic targets for LUAD with high abundance of PLK1.

RESULTS

PLK1 overexpression in LUAD correlates with poor patient survival.

To explore the expression of the families of *PLK*s in LUAD, we first used the TCGA database to compare the mRNA expression of *PLK*s in human LUAD samples with those of normal lung tissues. Compared with normal tissues, mRNA expression levels of *PLK1*,

PLK4 and *PLK5*, instead of *PLK2* and *PLK3*, were shown to be significantly enhanced in LUAD patients (fig. S1, A to E). Additionally, only the mRNA expressions of *PLK1* and *PLK4* significantly increased across the tumor stages of LUAD, while the rest of *PLK*s did not display significant difference in various tumor stages (fig. S1, F and G). Consistently, overexpressions of both *PLK1* and *PLK4*, other than other *PLK*s, were associated with limited survival rates (fig. S1, K to O).

To further explore the role of PLK1 in LUAD, we performed another large-scale analysis of *PLK1* expression using data obtained from Oncomine. Of note, patients with high *PLK1* expression had significantly lower survival probability, with a median survival of 25 months compared with 45.3 months for patients with lower *PLK1* expression (Fig. 1A). In addition, we analyzed the expression of *PLK1* among different pathological stages of lung cancer cases and identified a positive correlation between the expression of *PLK1* and tumor size (Fig. 1B). Furthermore, high *PLK1* expression correlated significantly with poorer tumor differentiation (Fig. 1C); compared with well-differentiated tumors, more *PLK1* was expressed in poorly differentiated tumors (Fig. 1C). Consistent with previous findings (21, 22, 24), our results indicate that *PLK1* overexpression promotes LUAD development by accelerating tumor cell growth and inducing dedifferentiation, which eventually leads to a reduced survival rate.

PLK1 overexpression accelerates the development of KP-mediated LUAD.

Activating mutations in KRAS are the most prevalent oncogenic driver in LUAD, and loss of p53 often cooperates with oncogenic KRAS to induce LUAD (25). From TCGA dataset, we found PLK1 overexpression correlated with KRAS mutations and co-mutations in *TP53* (fig. S1, P and Q). To investigate the role of PLK1 in LUAD development, we performed genetic crosses to incorporate a *Plk1* transgene into the KP mouse model, hereafter referred to as KPP (Fig. 2A). Upon validation that *Rosa26*$^{\text{LSL-}Plk1}$ was inserted into the genome of KP mice successfully (Fig. 2B), both cohorts were infected with adenovirus-expressing Cre (Ad-Cre) recombinase via intratracheal instillation to activate transgenes (Fig. 2C). We analyzed the mice at fixed time points and also performed a long-term analysis to assess the impact of PLK1 overexpression on overall survival. Magnetic resonance imaging (MRI) revealed significantly larger lung tumors (Fig. 2, D to F) in the KPP mice at 10 weeks post-Cre delivery, with the average tumor burden increased from 33.41% for the KP mice to 54.36% for the KPP mice (Fig. 2F). Then, fresh tissues were harvested for further analysis (Fig. 2G). Compared with normal lung tissues, the protein levels of PLK1 increased in KP tumors, but only slightly (fig. S2A). However, the protein amount of PLK1 was further enhanced in our KPP mouse model (Fig. 2, H and I), which facilitates studying the effect of PLK1 overexpression on LUAD. Upon PLK1 overexpression, the KPP tumors displayed more positive staining for phospho-Ser^{10} histone H3 (p-H3), suggesting increased tumor cell proliferation (Fig. 2, J and K). Histopathological review confirmed NSCLC (adenocarcinoma) histology of both cohorts (Fig. 2L). The KP cohort showed multiple foci of hyperchromatic tumor nodules comprised of papillary proliferations of atypical pneumocytes with increased eosinophilic cytoplasm and enlarged nuclei with irregular nuclear contours, consistent with a well-differentiated adenocarcinoma, papillary type (Fig. 2L). In contrast, the KPP cohort exhibited an increased overall tumor

burden, as well as formation of sheets and clusters with no overt glandular or papillary differentiation, consistent with a poorly differentiated adenocarcinoma (Fig. 2L). Of note, long-term analysis showed that the KPP cohort became moribund earlier, with 91 days of median survival compared with 113.5 days for the KP cohort (Fig. 2M), consistent with what we observed with human patients (Fig. 1A). Together, these data illustrate that PLK1 overexpression promotes the development of KP-mediated LUAD.

PLK1 overexpression results in increased *Ret* expression and enhanced MAPK pathway activity.

To understand how PLK1 overexpression promotes LUAD development, RNA sequencing (RNA-seq) analyses were performed to compare KP tumors with KPP tumors. The results showed significantly differential expression of 134 genes, of which 37 were upregulated and 97 were downregulated in KPP tumors (Fig. 3A and data file S1). Among these genes, *Ret* was an intriguing target for study because increased expression of wild-type RET is now being recognized to play a tumor-promoting role in many tumor types (26, 27). More importantly, the heat map in which genes were clustered by their expression patterns showed that *Ret* and *Plk1* were similarly altered (Fig. 3B), implying that *Ret* expression might be regulated by PLK1. Activation of RET is associated with stimulation of some important signaling pathways including RAS/extracellular signal-regulated kinase (ERK), phosphatidylinositol 3-kinase (PI3K)/AKT and c-Jun N-terminal kinase (JNK) pathway (27, 28). To identify gene sets and pathways enriched in the KPP tumors, we queried the 50 gene-set “Hallmark” gene signatures from MSigDB (29). Gene sets related to KRAS_SIGNALING_UP, PI3K_AKT_MTOR_SIGNALING and IL6_JAK_STAT3_SIGNALING were significantly enriched in the KPP group (fig. S3, A and B), suggesting that all the three pathways are more active in the KPP tumors than the KP tumors, consistent with the increased expression of *Ret*. Next, we tried to validate our findings obtained from the RNA-seq analyses. The enhanced expression of *Ret* upon PLK1 overexpression was confirmed by qRT-PCR (Fig. 3C). Also, immunoblots and IHC staining revealed higher protein levels of RET in the KPP tumors than the KP tumors (Fig. 3, D and E). However, we did not observe any significant change in the levels of its co-receptors or its ligand glial cell line-derived neurotrophic factor (GDNF) between the two cohorts (Fig. 3, F and G). Consistent with the increased abundance of RET, the abundance of phosphorylated RET (p-RET) at Tyr^{1086}, which is responsible for activation of both the MAPK and PI3K pathways, was also enhanced, concomitant with higher levels of p-ERK and p-AKT in the KPP tumors (Fig. 3E). KRAS-mutant cancer cell lines have been shown to have a greater dependency on MAPK signaling than others (30). Therefore, a transcriptional MAPK Pathway Activity Score (31) which includes 10 key downstream genes of the MAPK pathway was examined. Notably, PLK1 overexpression increased the mRNA levels of all the genes (Fig. 3H), implying the MAPK pathway is more active in the KPP tumors. Together, these data indicate that PLK1 overexpression cooperates with KP mutations to promote LUAD by increasing *Ret* expression.

RET promotes PLK1-overexpressing LUAD growth.

To understand how upregulated RET contributes to the development of LUAD tumors upon PLK1 overexpression, we established cell lines from three independent KP and KPP tumors,

termed KPc1 to 3 and KPPc1 to 3, respectively (Fig. 4A). PCR of genomic DNA confirmed complete recombination of the LSL-*Kras*^{G12D}, *Trp53*$^{fl/fl}$, and LSL-*Plk1* in each cell line (Fig. 4B). Immunoblot analysis verified that KPPc cells expressed higher protein levels of PLK1 and RET, as well as their active forms p-PLK1 and p-RET, than KPc cells (Fig. 4C). Also, the levels of p-ERK and p-AKT were enhanced in KPPc cells (Fig. 4D), an indication that both the MAPK and PI3K pathways are more active. Upon comparing the growth rates of the two cell lines, we found that KPPc cells formed larger oncospheres (Fig. 4, E and F), and exhibited higher plating efficiency in soft agar than did KPc cells (Fig. 4G). Moreover, assessment of the cell cycle distribution of the cell lines showed that a large proportion of KPc cells were arrested in S phase, whereas a great number of KPPc cells progressed into G2/M phase (Fig. 4, H to J), in line with the p-H3 levels of KP and KPP tumors (Fig. 2, J and K). Therefore, the molecular changes and transformed behavior displayed by KPc and KPPc cells are consistent with KP and KPP tumors in vivo, confirming that these cell lines can be used for further experimentation.

The advantage of the increased RET abundance was then assessed in these established cell models. We observed that GDNF stimulation resulted in strong RET autophosphorylation and activation of extracellular signal-regulated kinases 1 and 2 (ERK1/2) in KPPc cells, whereas GDNF had a weaker effect on KPc cells (Fig. 4K). We also investigated the cell growth rates of KPPc and KPc upon GDNF treatment. Consistent with the previous data (Fig. 4, F and G), KPPc cells exhibited a higher growth rate than that of KPc cells (Fig. 4K). Notably, GDNF accelerated the growth of both KPPc and KPc, but had a more profound effect on KPPc cells (Fig. 4L), implying that the enhanced RET level renders cells more sensitive to its ligand, which results in a growth advantage. To further confirm the role of RET, KPPc cells were transfected with shRNA targeting *Ret* and starved overnight. Upon knocking down *Ret* expression, KPPc cells exhibited lower levels of p-RET and p-ERK after GDNF stimulation (Fig. 4M). In addition, the loss of RET reduced the growth rate of KPPc in the presense of GDNF (Fig. 4N). Consistently, *Ret* shRNA-expressing allografts displayed smaller tumor sizes and lighter tumor weights after one month of growth (Fig. 4, O and P), coincident with a significant decrease in MAPK activity (Fig. 4, Q to S). We also used the pSECC lentivirus (32) for in vivo CRIPR/CAS9- knockout of *Ret* in KPP tumors (Fig. 4T). In line with our previous results, RET depletion in vivo inhibited tumor growth in the KPP mice with decreasing the activity of the MAPK pathway (Fig. 4, U to W), indicating that eliminating RET prevents the tumorigenic gain by PLK1 overexpression.

Elimination of PLK1 negatively affects KP-mediated lung tumors.

To further evaluate the role of PLK1 in LUAD development, we crossed conditional PLK1-knockout (*Plk1*$^{flox/flox}$) and KP mice to generate another tri-transgenic mouse model: KPO (Fig. 5A). After PCR validation of insertion of *Plk1*$^{flox/flox}$ into KP mice (Fig. 5B), lung tumorigenesis was initiated by intratracheal injection of Ad-Cre. At the 12th week after Ad-Cre infection, lung tumors from both KP and KPO mice were monitored by MRI. Compared with KP mice, the KPO mice displayed significantly reduced tumor burden (Fig. 5, C and D). Upon analysis of fresh tissues from both cohorts, we found that knockout of PLK1 appeared to markedly inhibit tumor growth and that the lungs appeared to be healthy (Fig. 5E). Although a few tumors were found among the KPO cohort, none of those tumors

had completely lost PLK1 (Fig. 5F), indicating PLK1 is required for KP-mediated LUAD tumorigenesis (33). To support this, KPc cells lacking PLK1 by siRNA-mediated repression (Fig. 5G) failed to form oncospheres in the 3D culture medium (Fig. 5H), which could not be rescued by subsequent overexpression of RET (fig. S4, A and B).

We then looked more closely at those KPO tumors that had retained some expression of PLK1. Immunoblotting revealed a reduction in PLK1 abundance in all the three KPO tumors (Fig. 5I). Notably, as PLK1 decreased, the abundance of both RET and p-RET were also reduced (Fig. 5, I and J). Furthermore, concomitant reduction of the activity of the MAPK pathway was observed in KPO tumors, manifested by decreased ERK1/2 phosphorylation (Fig. 5I). Together, these data suggest that PLK1 is required for tumorigenesis and confirm that *Ret* expression is likely to be regulated by PLK1 in KRAS/p53-mediated LUAD.

PLK1 regulates *Ret* expression through the phosphorylation of TTF-1.

Next, we investigated whether and, if so, how PLK1 might regulate *Ret* expression. First, we used shRNA to knock down PLK1 in KPPc cells. PLK1 knockdown led to reduced RET levels (Fig. 6A), as expected, but notably through decreasing its expression rather than affecting its protein stability (Fig. 6B and fig. S5). In addition, KPc cells exhibited increased levels of RET after Flag-PLK1 was stably expressed (Fig. 6C). These data suggest that RET is regulated by PLK1 in KP-mediated LUAD cells. Then, we treated KPPc with the ATP-competitive PLK1 inhibitor GSK461364. At micromolar concentrations, GSK46134 inhibited the growth of KPPc without inducing obvious late apoptosis (fig. S7, A to C). Upon the treatment, RET levels in KPPc gradually decreased in both dose-dependent (Fig. 6D) and time-dependent (Fig. 6E) manners, indicating that RET is regulated by PLK1 in a kinase activity-dependent manner.

Considering that PLK1 is a kinase, we reasoned that the regulation of *Ret* expression should be indirect. Thyroid transcription factor 1 (TTF-1, also known as NKX2-1) is reportedly a transcription factor for *RET* (34), so we reasoned that TTF-1 could be a mediator between PLK1 and RET. To test this hypothesis, we first performed immunoprecipitation experiments, and found PLK1 interacted with endogenous TTF-1 in KPPc cells (Fig. 6, F and G). We then sought to determine whether TTF-1 is a direct substrate of PLK1. When recombinant mouse TTF-1 and recombinant PLK1 were incubated in an in vitro kinase reaction, a robust incorporation of γ–^{32}P from ATP onto TTF-1 was detected; this was not observed in the presence of GSK461364 (Fig. 6H). To precisely identify which site of TTF-1 is phosphorylated by PLK1, we mutated all the serine/threonine sites that fully or approximately fit the PLK1 consensus phosphorylation motif: [D/N/E]-X-S/T-[F/Φ; no P]-[Φ/X] (35, 36). PLK1 was found to directly phosphorylate TTF-1 at Ser^{23} (Fig. 6I and S6), a site that is an ideal match for the optimal kinase motif of PLK1 and highly conserved across species (Fig. 6J) (35, 36).

To reveal how the phosphorylation of Ser^{23} affects RET, KPc cells were deprived of endogenous TTF-1 (Fig. 6K) and then were transfected with exogenous PLK1 and a non-phosphorylatable TTF-1 mutant, S23A. In contrast to what was observed in the presence of endogenous TTF-1 (Fig. 6C), the expression of S23A-TTF-1 prevented PLK1 from enhancing RET abundance (Fig. 6L). In KPPc cells deprived of endogenous TTF-1 (Fig.

6M), transfection with wild-type or a phosphomimetic (S23D) mutant TTF-1, but not S23A-TTF-1, increased the abundance of RET protein (Fig. 6N). To further dissect the mechanism, we cloned 3-kb promoter region of *Ret* into a luciferase reporter plasmid. Luciferase assay revealed a significant loss of S23A-TTF-1 from the *Ret* promoter region compared with WT-TTF-1 or S23D-TTF-1 (Fig. 6O). Moreover, ChIP-PCR were performed with KPPc cells to identify the binding site of TTF-1. Of note, the site P1, rather than P2 or P3, of the *Ret* promoter exhibited significant enrichment upon immunoprecipitation with TTF-1 antibody (Fig. 6, P and Q). However, this enrichment was significantly reduced when cells were treated with GSK461364 (Fig. 6R), indicating the importance of PLK1 phosphorylation on the regulation of TTF1's binding to the *Ret* promoter. Furthermore, both WT-TTF-1 and S23D-TTF-1 promoted the binding of TTF-1 to the *Ret* promoter, whereas S23A-TTF-1 did not (Fig. 6S). Finally, WT-TTF-1 and S23D-TTF-1 significantly accelerated proliferation of KPPc cells, whereas again S23A-TTF-1 did not (Fig. 6T). In summary, PLK1-mediated phosphorylation of TTF-1 at Ser^{23} promotes TTF-1 occupancy on the *Ret* promoter to stimulate *Ret* expression, thereby enhancing lung tumor cell growth.

Inhibition of either RET or PLK1 significantly improves the response of PLK1-overexpressing LUAD to trametinib.

Although tremendous effort has been put into developing drugs that targets the KRAS mutation, most KRAS mutants are still considered to be undruggable (37). Thus, inhibiting downstream of RAS, such as the MAPK pathway, might be an alternative approach. Trametinib, a MEK inhibitor, has been approved by the FDA to treat lung cancer (38). Of note, trametinib exhibited strong inhibition of KPc growth in vitro, but PLK1 overexpression rendered KP-mediated lung tumor cells resistant to the agent (Fig. 7, A to C). Given that the PLK1/TTF-1/RET axis acts upstream of the MAPK pathway, we tested whether the inhibitors targeting PLK1 or RET could improve trametinib's efficacy in inhibiting KPPc cells. Compared with single-agent treatment, both the pralsetinib/trametinib combination and the GSK461364/trametinib combination caused significantly greater reduction in two-dimensional colony formation (Fig. 7, D to G) and three-dimensional sphere formation of KPPc cells (Fig. 7, H and I). All the drugs inhibited their targets effectively at the indicated concentrations (fig. S7, D to F). Also, whereas single-agent treatment suppressed the level of p-ERK, the effect was markedly enhanced by simultaneous inhibition of RET or PLK1 (Fig. 7J). Furthermore, we evaluated the in vivo efficacy of the combination treatments by using KPP mice. 18 KPP mice at 8 weeks after Ad-Cre infection were randomized into 6 groups and underwent a 14-day treatment. As a single agent, pralsetinib or GSK461364 inhibited tumor growth relative to vehicle-treated controls but failed to elicit tumor regression in all the mice (Fig. 7, K and L). Although treatment of trametinib alone produced slight to moderate tumor regression, combination with pralsetinib or GSK461364 led to more profound tumor regression (Fig. 7, K and L). IHC staining against Ki-67 showed that the combination treatments inhibited tumor proliferation almost completely (Fig. 7, M and N). Notably, the tumors in the combination cohorts also displayed loss of nuclear expression of p-ERK (Fig. 7, O to R), confirming that the combination treatments were successful in inhibiting the MAPK pathway. Then, a long-term analysis was performed to evaluate whether the combination treatments could translate into survival benefits. The combination

of pralsetinib/trametinib successfully prolonged the survival of KKP mice with LUAD, but the GSK461364/trametinib combination couldn't (fig. S8A).

DISCUSSION

It is generally believed that increased PLK1 expression is oncogenic, as it has been documented in various human malignancies (39–45). In our analysis of GEO data, high *PLK1* mRNA expression correlates with poor tumor differentiation, a large tumor size, and a low survival rate in LUAD patients. In support of these data, association between a high abundance of PLK1 protein and advanced clinical stages is also observed in NSCLC patients (21). To study the function of PLK1 in LUAD, we generated the KPP mouse model in which PLK1 was increased specifically in the lung upon Cre expression. Compared with KP mice, the KPP mice displayed a lower survival rate, as well as larger tumors with poorer differentiation and a higher proliferation rate. This recapitulates the characteristics of human LUAD tumors harboring a high level of PLK1, suggesting that this mouse model is an ideal tool to study PLK1-overexpressing LUAD. In addition, we also knocked out PLK1 from KP mice. Although reduced compared to that in control tumors, the PLK1 protein was still present in all samples tested. Incomplete gene knockouts in transgenic mice have also been observed previously (46), which might be caused by inefficient Cre recombination of the transgenes (46, 47). Furthermore, we used in vitro experiments in which KP tumor cells were targeted with PLK1 siRNA, and found that this eliminated the development of tumor spheroids. Therefore, It is plausible that PLK1 is required for KP-mediated LUAD initiation, and that tumor cells without PLK1 are unable to grow (33, 48). All together, these data indicate that PLK1 is indeed required for LUAD tumorigenesis and that PLK1 plays a critical role in promoting LUAD development.

Although PLK1 is well known for its multiple roles in cell-cycle regulation, increasing evidence suggests that PLK1 might have many additional functions (19). Prior studies have showed that PLK1 positively regulates the MAPK pathway (49–51), but the underlying mechanisms remain elusive. In the current study, one major pathway we identified to be affected by PLK1 is RET signaling. Aberrant RET signaling, including RET overexpression, RET fusions and RET point mutations, is involved in various human cancers (lung, breast, thyroid) (52). Ligand-independent RET activation, through point mutation or rearrangement, was considered as oncogenic drivers in multiple cancers (26). However, ligand-mediated activation of wild-type RET is increasingly recognized to promote tumor growth (26). It is well known that KRAS mutations are the most frequent mutations in NSCLC patients and that NSCLC cell lines with KRAS mutations preferentially activate MAPK signaling (53). Therefore, the upregulation of RET induced by PLK1 cooperates with $KRAS^{G12D}$ to activate the MAPK pathway, eventually accelerating LUAD development.

TTF-1, a homeobox-containing transcription factor, plays an important role in the development of lung, thyroid and a restricted part of the brain (54). Emerging evidence suggests that TTF-1, as a double-edged sword, can have both pro- and anti-oncogenic functions in lung cancer (55). One possible reason is that activity of TTF-1 is context-dependent; interaction with other proteins, such as FOXA2, Smad3 and TAZ, is important for regulating its function (56–58). In addition, posttranslational modifications, including

acetylation and phosphorylation, can also affect its activity (59–61). For example, PKA phosphorylates TTF-1 at Thr^{9}, which activates its transcriptional function (60). In our study, we found that TTF-1 was phosphorylated by PLK1 at Ser^{23}, a site that is situated in the same activation domain as Thr^{9} (62). Consistently, we found that PLK1 phosphorylation of TTF-1 at Ser^{23} upregulated its transcriptional activity in regulating RET. Although a high level of TTF-1 is considered as an anti-oncogenic factor in *Kras*-driven primary lung tumors (63, 64), we observed that overexpression of TTF-1 in KPPc cells significantly accelerated tumor cell growth, which indicates that PLK1 prompts TTF-1 to exert its pro-oncogenic function. One reason for this is the phosphorylation, but other factors may also contribute. Therefore, further investigation is needed to identify whether overexpression of PLK1 affect other molecules which alter TTF-1's functional context.

Despite the development of several small molecule inhibitors of $KRAS^{G12C}$ (8–10), KRAS remains an elusive target for direct inhibitors (11), highlighting the importance of developing new therapies for KRAS-mutant lung cancer. Data from in vitro studies has showed that KRAS-mutant cancer cell lines have a greater dependency on MAPK signaling than on PI3K signaling (30). Furthermore, in a large-scale screening, MEK inhibitors were shown to be the most effective agents in cancer cell lines harboring KRAS mutations (65). Clinical trials of monotherapy with trametinib, a highly specific and potent MEK1/2 inhibitors, were undertaken in KRAS-mutant NSCLC patients. Its effect was limited (66), suggesting that more efforts are needed to identify subsets of patients not likely to respond to monotherapy and to develop trametinib-based combination treatment strategies. In our study, we demonstrated that PLK1 overexpression reduced the efficacy of trametinib, indicating that PLK1 might be a prognostic biomarker for trametinib resistance in patients. We propose combined RET and MEK inhibition or combined PLK1 and MEK inhibition as therapeutic strategies to treat PLK1-overexpressing tumors. We verified the efficacy of the pralsetinib/trametinib combination and the GSK461364/trametinib combination by both in vitro and in vivo experiments. Upon the combination treatments, cooperation between the mutated KRAS and PLK1 was abolished, eventually dramatically suppressing the MAPK pathway. These findings, together with previous reports (67, 68), further support a combination strategy targeting MEK to treat KRAS-mutant lung cancer.

MATERIALS AND METHODS

Mouse models

Rosa26$^{LSL\text{-}Plk1/+}$ mice have been described previously (69). *Plk1*$^{fl/fl}$ mice were a kind gift from Dr. Guillermo de Cárcer from Spanish National Cancer Research Centre (CNIO), Madrid, Spain (70). The loxP-STOP-loxP (LSL)-*Kras*^{G12D}; *p53*$^{fl/fl}$ (KP) mice were kindly provided by Dr. Andrea Kasinski from Purdue University, USA. Mixed groups of male and female mice were used in all experiments. For adenovirus studies, Ad5-CMV-Cre (Ad-Cre) was purchased from University of Iowa, and instilled into mice via intratracheal delivery at a viral titer of 2.5×10^{7} PFU per mouse according to the protocol by DuPage *et al.* (71). All animal experiments were approved by the University of Kentucky Animal Care and Use Committee.

Cell culture and cell lines

Mouse lung tumor cell lines were isolated from transgenic mice 12–14 weeks after Ad-Cre infection. All lung tumor cell lines were grown in RPMI 1640 medium plus 10% fetal bovine serum (FBS) and incubated in a humid atmosphere at 37°C with 5% CO_2. 293T cell line was purchased from ATCC, and grown in DMEM medium supplemented with 10% FBS in the same environment.

Antibodies and reagents

Antibodies against β-actin (8457), p-H3 (9714), RET (14556), p-MEK (9154), MEK (9122), p-AKT (4051), AKT (4691), H3 (9715), GAPDH (2118), and TTF-1 (12373) were from Cell Signaling Technology. Antibodies against p-ERK (sc7383), ERK (sc514302), GFRα−1 (sc271546) and GFRα−3 (sc-398618) were from Santa Cruz Biotechnology. Antibodies to Ki67 (ab16667) and TTF-1 (ab133737) for chromatin immunoprecipitation were from Abcam. Antibody to p-RET (orb304551) was from Biorbyt, and antibody to p-TTF-1 was from Sino Biological. Pralsetinib (S8716), trametinib (S2673), and GSK461364 (S2193) were from Selleckchem Chemicals Llc. GFRα−2 (PA5-115280), GFRα−4 (PA5-104239), and lipofectamine 2000 (11668019) were from Thermo Fisher Scientific. Mouse RET cDNA clone (MG57032-U) was from Sino Biological, murine TTF-1 cDNA clone (31271) was from Addgene, and recombinant TTF-1 protein (NKX2-1-10697M) was from Creative Biomart. shRNAs targeting *Ttf-1* (TRCN0000086263, TRCN0000086264), *Ret* (TRCN0000361385, TRCN0000368724), or *Plk1* (TRCN0000274592, TRCN0000274637), and siRNAs targeting *Plk1* (SASI_Mm01_00072214, SASI_Mm01_00072216) were all from Sigma.

Immunoblotting and immunoprecipitation (IP)

Upon harvest, cells were suspended with ice-cold RIPA buffer (Millipore, catalog no. 20–188) with protease and phosphatase inhibitors, and mixed on a rotator at 4 °C for 30 minutes, followed by measurement of protein concentration with Protein Assay Dye Reagent (Bio-Rad, catalog no. 5000006). For analysis, tumors were immediately snap frozen in liquid nitrogen and homogenized on ice in the mixed buffer described above. Equal amounts of protein from each sample were mixed with SDS loading buffer, resolved by SDS-PAGE, transferred to PVDF membranes, followed by incubation with appropriate primary and secondary antibodies. For immunoprecipitation, lysates were incubated with various antibodies in RIPA buffer mixed with Protein A/G magnetic Dynabeads (Invitrogen) at 4°C overnight, followed by three washes with 500 mM NaCl and three washes with 150 mM NaCl. All samples were resuspended and boiled, followed by IB to detect interactions between proteins.

Cell viability assay

Cells were dissociated, counted and plated in 50μL medium with ~2500 cells per well in 96-well plates. 50-μL medium with indicated treatments was added after 24 hours. All cells were treated for 48 hours, followed by incubation with the tetrazolium dye MTT (3-(4, 5-dimethylthiazol-2-yl)-2, 5-diphenyltetrazolium bromide) for 4 hours. After the purple formazan was dissolved in DMSO, absorbance at 570 nm was measured by a plate reader.

Quantitative RT-PCR (qRT-PCR) and RNA-sequencing (RNA-seq)

Total RNA was isolated from tumors or cells with the RNeasy® mini kit ((#74104, Qiagen) according to the manufacturer's instructions. cDNA was synthesized from 1-μg RNA (iScript cDNA synthesis kit (Bio-Rad)), followed by gene amplification with FastStart Universal SYBR Green (Roche Applied Science) and a Roche LightCycler 96 thermocycler (Roche Diagnostics Corp.). All individual reactions were performed in triplicate with all genes being normalized to β-actin. All data are presented as means ± SD. qRT-qPCR primers are listed in Supplementary Materials (table S1). For RNA-seq, total RNA was extracted from whole tumors with the same kit. Specifically, only one tumor was harvested from each mouse, and six mice were selected from either cohort (the KP cohort: 6 tumors; the KPP cohort: 6 tumors). All samples were sent to Novogene Biotechnology Company (CA, USA) for RNA quality assessment, RNAseq library construction, Illumina sequencing and data analysis. Readcount obtained from Gene Expression Analysis was used to do differential expression analysis. Gene expression data normalization and differential expression analysis were performed using the DESeq2 R package. Significantly up/downregulated genes were determined as fold change >= 2 and q-value < 0.05. GSEA was performed with GSEA version 4.1.0 (Broad Institute) with rank-ordered gene lists generated using all log-fold change values.

Magnetic resonance imaging (MRI)

MR images were obtained by the University of Kentucky Small Animal Magnetic Resonance Imaging facility. A Brucker ClinScan system that has 12 cm actively shielded gradients with slew rate of 6300 T/m/s and maximum strength of 630 mT/m was used. Animals were anesthetized with 2% v/v isoflurane in O_2 and then moved to the heated animal bed where anesthesia was set to 2%. Respiration rate was monitored via a pneumatic respiratory monitor (SA instruments). Images were taken with the 7T system with a 2×2 array coil with a 2D gradient echoT1-weighted sequences with parameters: 18 slices, TR = 170 ms, TE = 2.4 ms, α=38°, Navg=3, FOV 26 × 26 mm2, 1mm thickness, matrix size 256 × 256, for a voxel size of 0.102 × 0.102 × 1.0 mm, and gated to the animals' respiratory cycle to eliminate breathing motion artifacts. Tumor was quantified by 3D-Slicer software (http://www.slicer.org).

Analysis of LUAD data from the ONCOMINE and TCGA datasets

Data analysis was conducted by Biostatistics & Bioinformatics Shared Resource Facility, Markey Cancer Center in University of Kentucky. GEP data used in this study are from Direcor's Challenge Consortium for the Molecular Classification of Lung Adenocarcinoma (72), which was downloaded from the Oncomine database. TCGA lung adenocarcinoma patient data were obtained from The Cancer Genome Atlas (TCGA, https://cancergenome.nih.gov/); the complete Clinical Data set was collected from level 2, and the RNA-seq data were collected from Level 3 (for Segmented or Interpreted Data, IllumninaHiSeq_RNASeqV2 of TCGA). All statistical analyses and corresponding figures were conducted in R-4.0.0. The Kaplan-Meier method and the log rank test were used to compare survival time and tumor progression between high and low gene expression subgroups with median chosen as threshold. ANOVA was used to compare the gene

expressions among the three subgroups stratified by stages, and Tukey's HSD method was used to adjust for multi-group comparisons.

Histology and immunohistochemistry (IHC)

Mouse tissues or tumors were fixed in 10% neutral-buffered formalin for 24 hours, and then transferred to 70% ethanol, embedded in paraffin and sectioned at 4–5 μm. H&E staining was performed by the Biospecimen Procurement & Translational Pathology Shared Resource Facility (BPTP SRF) of the University of Kentucky Markey Cancer Center, and stained slides were scanned with an Epson scanner. IHC staining was performed with the VECTASTAIN® Elite® ABC Universal PLUS Kit (PK-8200) from Vector Laboratories, following the manufacturer's instructions. Staining was visualized with brown DAB substrate and the counterstain was Harris's hematoxylin.

Enzyme-linked immunosorbent assay (ELISA)

Tumor tissues were minced into small pieces and rinced in ice cold phosphate-buffered saline (PBS). Tumor pieces were weighed and homogenized in PBS (tumor weight (g): PBS (mL) volume=1:9) with 1× Protease Inhibitor Cocktail, followed by the addition of Triton X-100. The homogenates were then centrifuged for 10 minutes at 5000×g at 4°C to get the supernatants. Tissue concentrations of GDNF were determined on these supernatants using an ELISA kit (MBS2507522, MyBioSource) according to the manufacturer's instruction.

Tumor cell 3D culture

MTEC/Plus medium was prepared by addition of 1x Insulin/transferrin/selenium mixture (Corning), 1x penicillin/streptomycin, 10% FBS, 0.1μg/mL cholera toxin (Sigma, #C8052), 10μg/mL Insulin (Sigma, #I-6634), 4mM L-glutamine, 12.5μg/mL bovine pituitary extract (Invitrogen, #13028-014), 25 ng/mL mEGF (Invitrogen, #53003-018) and 25 ng/mL rmFGF2 (R+D Systems, #3139-FB/CF) into DMEM/F12 medium. Tumor cells (~2500) were dissociated, resuspended in MTEC/Plus medium, mixed 1:1 with growth factor-reduced Matrigel (Coring), and seeded in a 24-well transwell insert (Corning, #CLS3470). The lower chamber was filled with MTEC/Plus medium, which was refreshed every other day. Dispase (Corning, #42613-33-2) was used for spheroids passage. After incubation at 37°C for 2 hours, the spheroids were collected into a tube for passage or for other purposes.

Flow cytometry analysis

To identify apoptotic cells, staining with a 7-AAd and Annexin-V kit (Biolegend, #640992) was performed according to the manufacturer's instruction. For cell cycle analysis, cells were harvested by trypsinization, treated with 70% ethanol for fixation, washed with ice cold 1X PBS twice, and stained with DNA stain propidium iodide (PI) at a final concentration of 50μg/mL at 37 °C for 1 hour. Cells were analyzed by CytoFLEX and FlowJo software.

Allograft model

KPPc cells (2×10^6) stably transfected with control or *Ret* -targeting shRNA were mixed with Matrigel (Collaborative Biomedical Products), and the mixture was injected subcutaneously into the right flank of the NSG mouse. Tumor volumes were measured every three days

by a caliper, and calculated from the formula V = L × W2/2 (where V is volume [cubic millimeters], L is length [millimeters], and W is width [millimeters]). All the mice were sacrificed 30 days after tumor cell injection for measurement of tumor weight and histopathologic and molecular analysis.

Lentiviral production

Lentiviruses were produced by transfecting 293T cells with lentiviral backbone constructs and packaging vectors (delta8.2 and VSVG) using TransIT®-LT1 transfection reagent (MIR2300, Mirus Bio). Lentiviruses were collected 48 hours post-transfection, ultracentrifuged at 25000 r.p.m. for 90 minutes, and resuspended in OptiMEM (Gibco). Lentiviruses' titers were determined using qPCR Lentivirus Titer Kit (LV900, Applied Biological Materials Inc).

For sgRNA cloning, the pSECC plasmid (#60820) was digested by BsmBI, and ligated with BsmBI-compatible pre-annealed oligo-nucleatides. The following sequences were used for CRISPR-knockout strategies: sgRet #3, GATGAAAGGGTACTGACCAT; sgRet #4, TTCGCCTGGCAGATCTCGAG. pSECC-sgTomato (#138661) was ordered from Addgene.

Kinase assay

In vitro kinase assays were conducted with 2 μM substrate, 0.5 μM PLK1 kinase, TBMD buffer (2 mM EGTA, 20 mM p-nitrophenyl phosphate, 10 mM $MgCl_2$, 50 mM Tris [pH 7.5], 0.5 mM sodium vanadate) and 10 μCi of [γ-^{32}P] ATP. The reaction mixture was incubated at 30 °C for 30 minutes, followed by SDS-PAGE. The gels were stained with Coomassie brilliant blue, dried and subjected to autoradiography.

Luciferase assay

Lipofectamine 2000 (Invitrogen) was used to transfect tumor cells with plasmids according to the manufacturer's instructions. Tumor cells were planted in a 24-well plate, and then transfected with 0.1 μg reporter plasmids containing the sequence of interest, as well as 5 ng of an internal control plasmid, pRL-TK. For the expression of transcription factors of interest, 0.6 μg of plasmid was transfected into the tumor cells. Luciferase activity was assayed after 48 hours of transfection with the dual luciferase reporter assay system (Promega). The firefly luciferase activities were corrected by the corresponding *Renilla* luciferase activities and presented as means ± SD.

Clonogenic assay

Tumor cells (~500) were seeded in 6-well plates with 2 ml RPMI 1640 supplemented with 10% FBS. After 7 days, the colonies were fixed by 10% formalin and stained with 5% crystal violet. Colony numbers were counted with Image J software.

Chromatin immunoprecipitation (ChIP) assay

ChIP assay was performed by using a commercial kit (Millipore, #17-10085) following the manufacturer's instruction. TTF-1 binding sites were predicted by JASPAR 2022 (73), and the PCR generated 100–200 bp products from the *Ret* proximal (< 2,000 bp) promoter containing sites. Antibodies against TTF-1 (ab133737) was purchased

from Abcam. The primers used were: P1, gaatcacaaacaagcccaacaggac (forward), cctccagtctctggacgcgaa (reverse); P2, acagggtaggcagccct (forward), agccagacgaatggagctacag (reverse); P3, ctgtgtcacatgctattccgctg(forward), gatgctggcagcccatcac (reverse).

Statistical analysis

Statistical analysis and graph production were performed using GraphPad Prism 6 software (GraphPad Software USA). Numerical data was analyzed using the student's *t* test or one-way ANOVA with Tukey's HSD post hoc analysis. The detailed methods for statistical test are described in the corresponding figure legends. Statistical significance was defined as $P < 0.05$. All numerical data are presented as means ± SD. All experiments were performed a minimum of three times independently.

Supplementary Material

Refer to Web version on PubMed Central for supplementary material.

Acknowledgements:

We thank Dr. Guillermo de Cárcer (Spanish National Cancer Research Centre) and Dr. Andrea Kasinski (Purdue University) for providing the transgenic mice.

Funding:

NIH R01 CA157429 (X. Liu), R01 CA196634 (X. Liu), R01 CA264652 (X. Liu), R01 CA256893 (X. Liu). This research was also supported by the Biospecimen Procurement & Translational Pathology, Biostatistics and Bioinformatics, Flow Cytometry and Immune Monitoring Shared Resources of the University of Kentucky Markey Cancer Center (P30CA177558).

Data and Materials Availability:

The RNA-seq data are deposited to Gene Expression Omnibus under the SuperSeries accession number GSE206644. All other data necessary for interpreting the study are presented in the main paper or supplementary materials.

REFERENCES AND NOTES

1. Siegel RL, Miller KD, Fuchs HE, Jemal A, Cancer statistics, 2022. CA Cancer J Clin 72, 7–33 (2022). [PubMed: 35020204]
2. Roman M et al. , KRAS oncogene in non-small cell lung cancer: clinical perspectives on the treatment of an old target. Mol Cancer 17, 33 (2018). [PubMed: 29455666]
3. Griffin R, Ramirez RA, Molecular Targets in Non-Small Cell Lung Cancer. Ochsner J 17, 388–392 (2017). [PubMed: 29230123]
4. Agalioti T, Giannou AD, Stathopoulos GT, Pleural involvement in lung cancer. J Thorac Dis 7, 1021–1030 (2015). [PubMed: 26150915]
5. Shames DS II Wistuba, The evolving genomic classification of lung cancer. J Pathol 232, 121–133 (2014). [PubMed: 24114583]
6. Zappa C, Mousa SA, Non-small cell lung cancer: current treatment and future advances. Transl Lung Cancer Res 5, 288–300 (2016). [PubMed: 27413711]
7. Baumgart A et al. , Opposing role of Notch1 and Notch2 in a Kras(G12D)-driven murine non-small cell lung cancer model. Oncogene 34, 578–588 (2015). [PubMed: 24509876]
8. Canon J et al. , The clinical KRAS(G12C) inhibitor AMG 510 drives anti-tumour immunity. Nature 575, 217–223 (2019). [PubMed: 31666701]

9. Janes MR et al. , Targeting KRAS Mutant Cancers with a Covalent G12C-Specific Inhibitor. Cell 172, 578–589 e517 (2018). [PubMed: 29373830]
10. Lito P, Solomon M, Li LS, Hansen R, Rosen N, Allele-specific inhibitors inactivate mutant KRAS G12C by a trapping mechanism. Science 351, 604–608 (2016). [PubMed: 26841430]
11. Singh H, Longo DL, Chabner BA, Improving Prospects for Targeting RAS. J Clin Oncol 33, 3650–3659 (2015). [PubMed: 26371146]
12. Cucurull M et al. , Targeting KRAS in Lung Cancer Beyond KRAS G12C Inhibitors: The Immune Regulatory Role of KRAS and Novel Therapeutic Strategies. Front Oncol 11, 793121 (2021). [PubMed: 35096591]
13. Seki A, Coppinger JA, Jang CY, Yates JR, Fang G, Bora and the kinase Aurora a cooperatively activate the kinase Plk1 and control mitotic entry. Science 320, 1655–1658 (2008). [PubMed: 18566290]
14. Golsteyn RM, Mundt KE, Fry AM, Nigg EA, Cell cycle regulation of the activity and subcellular localization of Plk1, a human protein kinase implicated in mitotic spindle function. J Cell Biol 129, 1617–1628 (1995). [PubMed: 7790358]
15. Elowe S, Hummer S, Uldschmid A, Li X, Nigg EA, Tension-sensitive Plk1 phosphorylation on BubR1 regulates the stability of kinetochore microtubule interactions. Genes Dev 21, 2205–2219 (2007). [PubMed: 17785528]
16. Lane HA, Nigg EA, Antibody microinjection reveals an essential role for human polo-like kinase 1 (Plk1) in the functional maturation of mitotic centrosomes. J Cell Biol 135, 1701–1713 (1996). [PubMed: 8991084]
17. Neef R et al. , Phosphorylation of mitotic kinesin-like protein 2 by polo-like kinase 1 is required for cytokinesis. J Cell Biol 162, 863–875 (2003). [PubMed: 12939256]
18. Schmidt A et al. , Xenopus polo-like kinase Plx1 regulates XErp1, a novel inhibitor of APC/C activity. Genes Dev 19, 502–513 (2005). [PubMed: 15713843]
19. Liu XS, Song B, Liu X, The substrates of Plk1, beyond the functions in mitosis. Protein Cell 1, 999–1010 (2010). [PubMed: 21153517]
20. Strebhardt K, Multifaceted polo-like kinases: drug targets and antitargets for cancer therapy. Nat Rev Drug Discov 9, 643–660 (2010). [PubMed: 20671765]
21. Wang ZX et al. , Overexpression of polo-like kinase 1 and its clinical significance in human non-small cell lung cancer. Int J Biochem Cell Biol 44, 200–210 (2012). [PubMed: 22064247]
22. Li H et al. , The clinical and prognostic value of polo-like kinase 1 in lung squamous cell carcinoma patients: immunohistochemical analysis. Biosci Rep 37, (2017).
23. Stratmann JA, Sebastian M, Polo-like kinase 1 inhibition in NSCLC: mechanism of action and emerging predictive biomarkers. Lung Cancer (Auckl) 10, 67–80 (2019). [PubMed: 31308774]
24. Zeng Y et al. , Analyses of expressions and prognostic values of Polo-like kinases in non-small cell lung cancer. J Cancer Res Clin Oncol 146, 2447–2460 (2020). [PubMed: 32627077]
25. Skoulidis F, Heymach JV, Co-occurring genomic alterations in non-small-cell lung cancer biology and therapy. Nat Rev Cancer 19, 495–509 (2019). [PubMed: 31406302]
26. Mulligan LM, GDNF and the RET Receptor in Cancer: New Insights and Therapeutic Potential. Front Physiol 9, 1873 (2018). [PubMed: 30666215]
27. Mulligan LM, RET revisited: expanding the oncogenic portfolio. Nat Rev Cancer 14, 173–186 (2014). [PubMed: 24561444]
28. Takahashi M, The GDNF/RET signaling pathway and human diseases. Cytokine Growth Factor Rev 12, 361–373 (2001). [PubMed: 11544105]
29. Liberzon A et al. , The Molecular Signatures Database (MSigDB) hallmark gene set collection. Cell Syst 1, 417–425 (2015). [PubMed: 26771021]
30. Ihle NT et al. , Effect of KRAS oncogene substitutions on protein behavior: implications for signaling and clinical outcome. J Natl Cancer Inst 104, 228–239 (2012). [PubMed: 22247021]
31. Wagle MC et al. , A transcriptional MAPK Pathway Activity Score (MPAS) is a clinically relevant biomarker in multiple cancer types. NPJ Precis Oncol 2, 7 (2018). [PubMed: 29872725]
32. Sanchez-Rivera FJ et al. , Rapid modelling of cooperating genetic events in cancer through somatic genome editing. Nature 516, 428–431 (2014). [PubMed: 25337879]

33. Liu X, Lei M, Erikson RL, Normal cells, but not cancer cells, survive severe Plk1 depletion. Mol Cell Biol 26, 2093–2108 (2006). [PubMed: 16507989]
34. Leon TY et al. , Transcriptional regulation of RET by Nkx2–1, Phox2b, Sox10, and Pax3. J Pediatr Surg 44, 1904–1912 (2009). [PubMed: 19853745]
35. Alexander J et al. , Spatial exclusivity combined with positive and negative selection of phosphorylation motifs is the basis for context-dependent mitotic signaling. Sci Signal 4, ra42 (2011). [PubMed: 21712545]
36. Kettenbach AN et al. , Quantitative phosphoproteomics identifies substrates and functional modules of Aurora and Polo-like kinase activities in mitotic cells. Sci Signal 4, rs5 (2011). [PubMed: 21712546]
37. Liu P, Wang Y, Li X, Targeting the untargetable KRAS in cancer therapy. Acta Pharm Sin B 9, 871–879 (2019). [PubMed: 31649840]
38. Halliday PR, Blakely CM, Bivona TG, Emerging Targeted Therapies for the Treatment of Non-small Cell Lung Cancer. Curr Oncol Rep 21, 21 (2019). [PubMed: 30806814]
39. Weichert W et al. , Polo-like kinase 1 is overexpressed in prostate cancer and linked to higher tumor grades. Prostate 60, 240–245 (2004). [PubMed: 15176053]
40. Schmit TL, Zhong W, Nihal M, Ahmad N, Polo-like kinase 1 (Plk1) in non-melanoma skin cancers. Cell Cycle 8, 2697–2702 (2009). [PubMed: 19652546]
41. Feng YB et al. , Overexpression of PLK1 is associated with poor survival by inhibiting apoptosis via enhancement of survivin level in esophageal squamous cell carcinoma. Int J Cancer 124, 578–588 (2009). [PubMed: 19004025]
42. Jang YJ, Kim YS, Kim WH, Oncogenic effect of Polo-like kinase 1 expression in human gastric carcinomas. Int J Oncol 29, 589–594 (2006). [PubMed: 16865274]
43. Kneisel L et al. , Expression of polo-like kinase (PLK1) in thin melanomas: a novel marker of metastatic disease. J Cutan Pathol 29, 354–358 (2002). [PubMed: 12135466]
44. Shi W et al. , Significance of Plk1 regulation by miR-100 in human nasopharyngeal cancer. Int J Cancer 126, 2036–2048 (2010). [PubMed: 19739117]
45. Takahashi T et al. , Polo-like kinase 1 (PLK1) is overexpressed in primary colorectal cancers. Cancer Sci 94, 148–152 (2003). [PubMed: 12708489]
46. Bowman BM et al. , Phosphorylation of FADD by the kinase CK1alpha promotes KRASG12D-induced lung cancer. Sci Signal 8, ra9 (2015). [PubMed: 25628462]
47. Zheng B, Sage M, Sheppeard EA, Jurecic V, Bradley A, Engineering mouse chromosomes with Cre-loxP: range, efficiency, and somatic applications. Mol Cell Biol 20, 648–655 (2000). [PubMed: 10611243]
48. Liu X, Erikson RL, Polo-like kinase (Plk)1 depletion induces apoptosis in cancer cells. Proc Natl Acad Sci U S A 100, 5789–5794 (2003). [PubMed: 12732729]
49. Dang SC et al. , PLK1 as a potential prognostic marker of gastric cancer through MEK-ERK pathway on PDTX models. Onco Targets Ther 11, 6239–6247 (2018). [PubMed: 30288059]
50. Jiang S, Tang DD, Plk1 regulates MEK1/2 and proliferation in airway smooth muscle cells. Respir Res 16, 93 (2015). [PubMed: 26242183]
51. Wu J, Ivanov AI, Fisher PB, Fu Z, Polo-like kinase 1 induces epithelial-to-mesenchymal transition and promotes epithelial cell motility by activating CRAF/ERK signaling. Elife 5, (2016).
52. Plaza-Menacho I, Mologni L, McDonald NQ, Mechanisms of RET signaling in cancer: current and future implications for targeted therapy. Cell Signal 26, 1743–1752 (2014). [PubMed: 24705026]
53. Ricciuti B et al. , Targeting the KRAS variant for treatment of non-small cell lung cancer: potential therapeutic applications. Expert Rev Respir Med 10, 53–68 (2016). [PubMed: 26714748]
54. Stanfel MN, Moses KA, Schwartz RJ, Zimmer WE, Regulation of organ development by the NKX-homeodomain factors: an NKX code. Cell Mol Biol (Noisy-le-grand) Suppl 51, OL785–799 (2005).
55. Yamaguchi T, Hosono Y, Yanagisawa K, Takahashi T, NKX2–1/TTF-1: an enigmatic oncogene that functions as a double-edged sword for cancer cell survival and progression. Cancer Cell 23, 718–723 (2013). [PubMed: 23763999]

56. Li C et al. , Transforming growth factor-beta inhibits pulmonary surfactant protein B gene transcription through SMAD3 interactions with NKX2.1 and HNF-3 transcription factors. J Biol Chem 277, 38399–38408 (2002). [PubMed: 12161428]
57. Minoo P et al. , Physical and functional interactions between homeodomain NKX2.1 and winged helix/forkhead FOXA1 in lung epithelial cells. Mol Cell Biol 27, 2155–2165 (2007). [PubMed: 17220277]
58. Park KS et al. , TAZ interacts with TTF-1 and regulates expression of surfactant protein-C. J Biol Chem 279, 17384–17390 (2004). [PubMed: 14970209]
59. Missero C, Pirro MT, Di Lauro R, Multiple ras downstream pathways mediate functional repression of the homeobox gene product TTF-1. Mol Cell Biol 20, 2783–2793 (2000). [PubMed: 10733581]
60. Yan C, Whitsett JA, Protein kinase A activation of the surfactant protein B gene is mediated by phosphorylation of thyroid transcription factor 1. J Biol Chem 272, 17327–17332 (1997). [PubMed: 9211870]
61. Yang L, Yan D, Bruggeman M, Du H, Yan C, Mutation of a lysine residue in a homeodomain generates dominant negative thyroid transcription factor 1. Biochemistry 43, 12489–12497 (2004). [PubMed: 15449938]
62. Silberschmidt D et al. , In vivo role of different domains and of phosphorylation in the transcription factor Nkx2–1. BMC Dev Biol 11, 9 (2011). [PubMed: 21345181]
63. Maeda Y et al. , Kras(G12D) and Nkx2–1 haploinsufficiency induce mucinous adenocarcinoma of the lung. J Clin Invest 122, 4388–4400 (2012). [PubMed: 23143308]
64. Snyder EL et al. , Nkx2–1 represses a latent gastric differentiation program in lung adenocarcinoma. Mol Cell 50, 185–199 (2013). [PubMed: 23523371]
65. Garnett MJ et al. , Systematic identification of genomic markers of drug sensitivity in cancer cells. Nature 483, 570–575 (2012). [PubMed: 22460902]
66. Blumenschein GR Jr. et al. , A randomized phase II study of the MEK1/MEK2 inhibitor trametinib (GSK1120212) compared with docetaxel in KRAS-mutant advanced non-small-cell lung cancer (NSCLC)dagger. Ann Oncol 26, 894–901 (2015). [PubMed: 25722381]
67. Engelman JA et al. , Effective use of PI3K and MEK inhibitors to treat mutant Kras G12D and PIK3CA H1047R murine lung cancers. Nat Med 14, 1351–1356 (2008). [PubMed: 19029981]
68. Gandara DR et al. , A Phase 1/1b Study Evaluating Trametinib Plus Docetaxel or Pemetrexed in Patients With Advanced Non-Small Cell Lung Cancer. J Thorac Oncol 12, 556–566 (2017). [PubMed: 27876675]
69. Li Z et al. , Polo-like kinase 1 (Plk1) overexpression enhances ionizing radiation-induced cancer formation in mice. J Biol Chem 292, 17461–17472 (2017). [PubMed: 28900036]
70. Wachowicz P, Fernandez-Miranda G, Marugan C, Escobar B, de Carcer G, Genetic depletion of Polo-like kinase 1 leads to embryonic lethality due to mitotic aberrancies. Bioessays 38 Suppl 1, S96–S106 (2016). [PubMed: 27417127]
71. DuPage M, Dooley AL, Jacks T, Conditional mouse lung cancer models using adenoviral or lentiviral delivery of Cre recombinase. Nat Protoc 4, 1064–1072 (2009). [PubMed: 19561589]
72. Director's A Challenge Consortium for the Molecular Classification of Lung et al., Gene expression-based survival prediction in lung adenocarcinoma: a multi-site, blinded validation study. Nat Med 14, 822–827 (2008). [PubMed: 18641660]
73. Castro-Mondragon JA et al. , JASPAR 2022: the 9th release of the open-access database of transcription factor binding profiles. Nucleic Acids Res 50, D165–D173 (2022). [PubMed: 34850907]

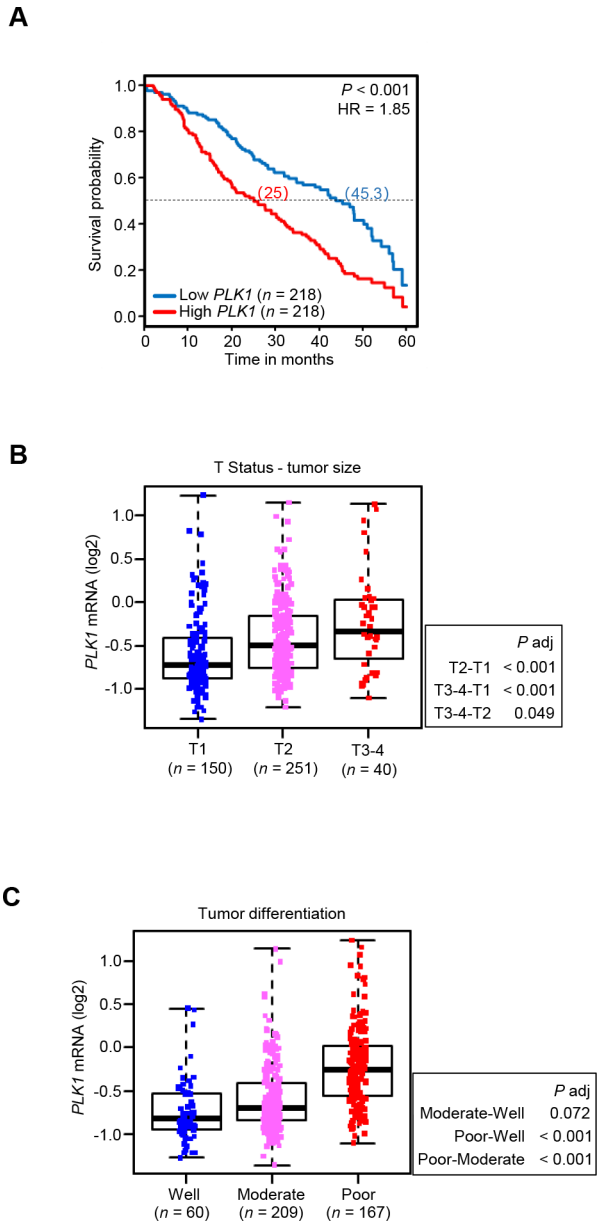

Fig.1. Overexpression of PLK1 correlates with low survival rate of LUAD patients, increased tumor size, and poor differentiation.

(**A**) *PLK1* expression versus the survival rate of LUAD patients in data from Oncomine and Director's Challenge Consortium for the Molecular Classification of LUAD. The number of patients (*n*) in each grouping is noted in the graph. The median split was used to dichotomize the continuous expression levels of *PLK1. P* values were calculated with log-rank test. (**B and C**) The expression of *PLK1* mRNA in T3-4 stage tumors compared with that in T1 or T2 stage tumors (B) and in poorly differentiated tumors compared with that in well-differentiated or moderately differentiated tumors (C), from the data sets noted in (A). *P* values determined by ANOVA with Tukey's HSD adjustment for multi-group comparisons.

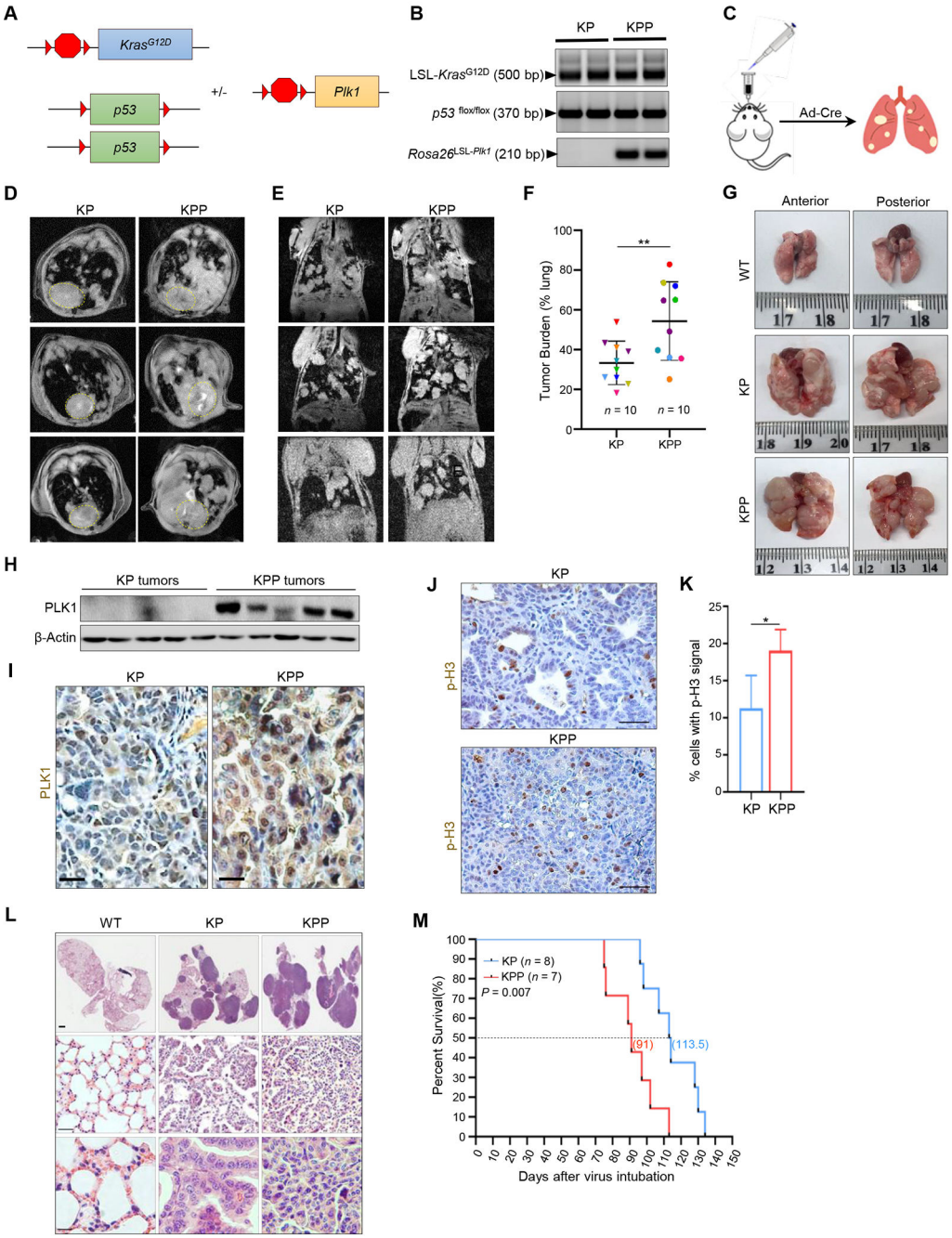

Fig.2. Overexpression of PLK1 promotes LUAD development.

(**A and B**) Schematic showing the crossing strategy (red triangles: loxP sites; red octagons: STOP cassettes), confirmed by PCR analysis of 50 ng of mouse genomic DNA (B). A representative of three experiments is shown. (**C**) Schematic showing the intratracheal inhalation of adenovirus-expressing Cre (Ad-Cre). (**D** and **E**) Representative axial and coronal MR images (D and E) and tumor burden (F) of the thorax regions from KP and KPP mice, each $n = 10$, 10 weeks after infection with Ad-Cre. Hearts are outlined with yellow circles. Data are means ± SD. $^{**}P < 0.01$ by unpaired Student's t test. (**G**) Representative

photographs of the lungs from wild-type (WT, $n = 3$), KP and KPP mice ($n = 10$) 12 weeks after Ad-Cre infection. (**H and I**) Immunoblotting and IHC analysis, respectively, of PLK1 abundance in a representative 5 (H) or 4 (I) tumors from KP and KPP mice. Scale bars: 200 μm. (**J** and **K**) IHC staining analysis of phospho-histone H3 (Ser^{10}) positivity in primary tumors from KP and KPP mice. Scale bars: 250 μm. Data are means ± SD from $n = 4$ mice each. $*P < 0.05$ by unpaired Student's *t* test. (**L**) H&E-stained sections of wild-type, KP and KPP tumors, each representative of four. Scale bars: 1mm, 250 μm, and 100 μm. (**M**) Survival rates of the KP and KPP mice, $n = 8$ and 7, respectively. *P* value by the log-rank test.

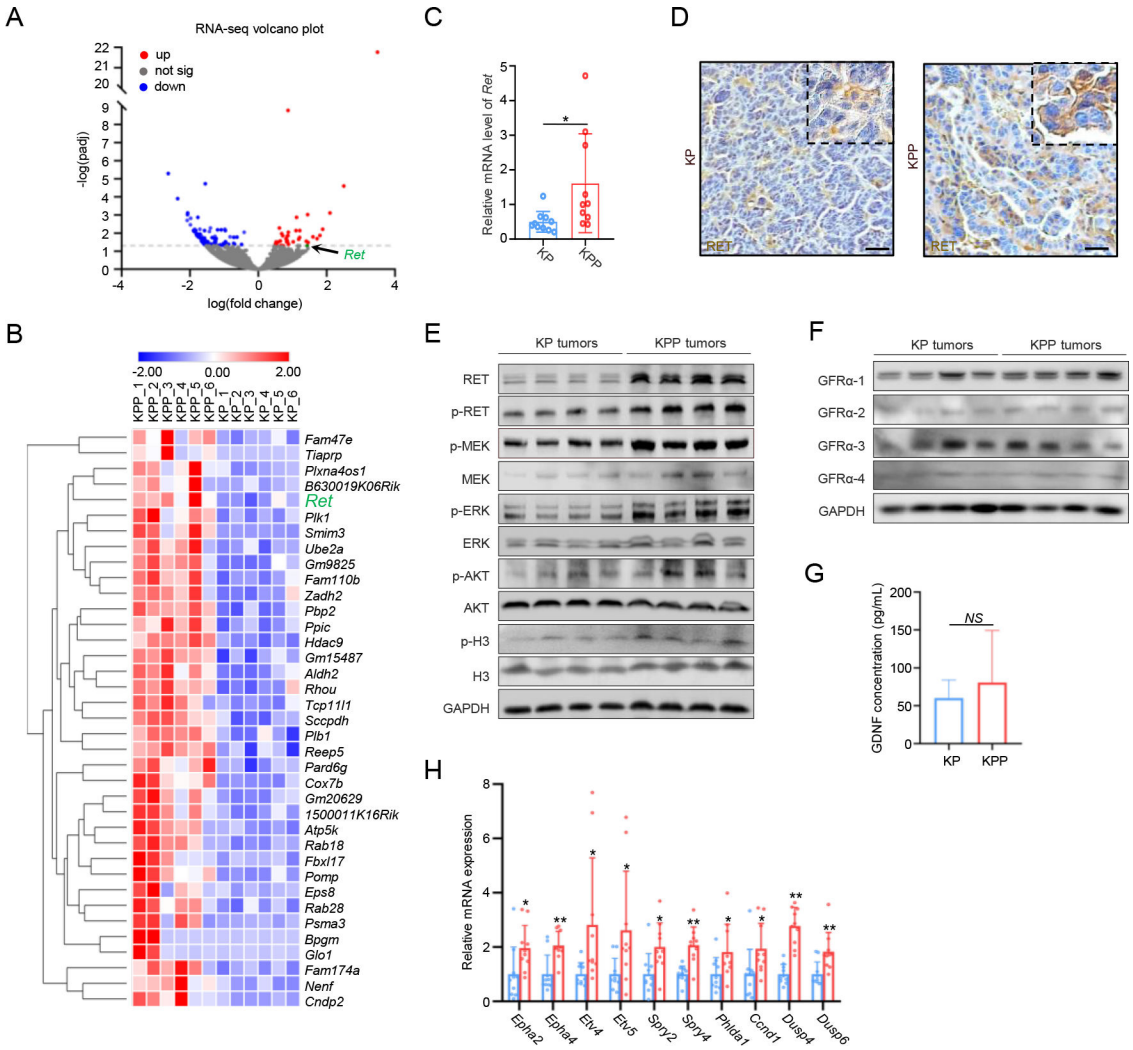

Fig.3. *Ret* expression is enhanced upon PLK1 overexpression.

(**A**) Volcano plot of significantly differentially expressed genes in KPP tumors relative to KP tumors. *Ret* is noted. Adjusted *P* value < 0.05. (**B**) Heat map of the 37 genes from (A) that were significantly upregulated upon PLK1 overexpression in primary tumors. Six primary tumors from either cohort were selected for analysis. The clustering method is based on the similarity of the gene expression; blue denotes low expression, and red denotes high expression. *Ret* is highlighted in green. (**C**) qRT-PCR of 10 KP tumors and 10 KPP tumors for validation of *Ret* expression. (**D**) IHC staining for RET in KP and KPP tumors, representative of four each. Scale bars: 100 μm. (**E** and **F**) Western blots on single primary KP and KPP tumor lysates from four mice each. (**G**) GDNF concentrations in 10 KP and 10 KPP tumors determined by ELISA. (**H**) qRT-PCR analysis of 10 target genes of the MAPK pathway in 10 KPP tumors (red) versus 10 KP tumors (blue). In (C, G, and H), data are means ± SD. **P* < 0.05, ***P* < 0.01, and *NS* not significant by unpaired Student's *t* test.

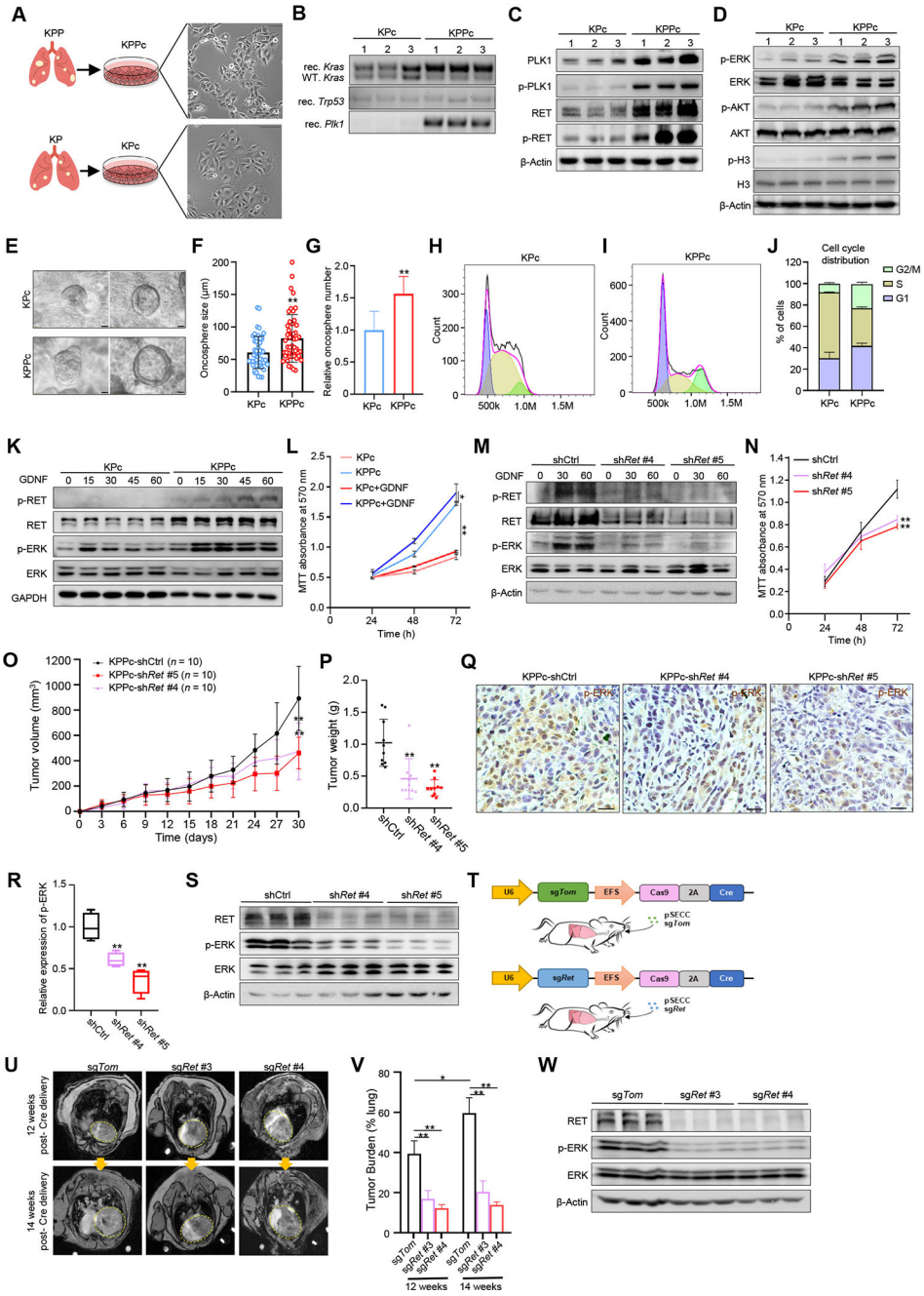

Fig.4. promotes LUAD cell proliferation by upregulating *Ret* expression.

(**A**) Schematic showing the establishment of LUAD cell lines. (**B**) PCR of genomic DNA from three independent KPc and KPPc cell lines (denoted by 1, 2, and 3). Cre-mediated recombination of LSL-Kras^{G12D}, Trp53$^{fl/fl}$, and Rosa26$^{LSL-Plk1}$ alleles. Rec., recombined; WT, wild-type. (**C** and **D**) Immunoblotting of the 3 KPc and 3 KPPc cell lines for the indicated proteins. (**E** to **G**) Micrographs of KPc and KPPc cells in soft agar (scale bars, 20 μm; E) and corresponding oncosphere size (diameter; F) and number (G). $n = 50$ oncospheres each; (**H** to **J**) Cell-cycle analysis by PI staining and flow cytometry of KPc

(H) and KPPc (I) cells, and quantification of cell-cycle phase distribution in each (J). n = 3 experiments. (**K**) Immunoblotting of lysates from KPc and KPPc cells starved overnight then treated with GDNF (20 ng/ml) for the indicated time. Blots are representative of three experiments. (**L**) MTT cell viability assay of untreated and GDNF-treated KPc and KPPc cells. GDNF, 20 ng/ml. n = 3 experiments each performed in triplicate. (**M**) Western blotting in KPPc cells stably transfected with one of two lentiviral shRNAs targeting *Ret* (sh*Ret* #4 and sh*Ret* #5) or a non-target control (shCtrl), starved overnight, and treated with GDNF (20 ng/ml) for the indicated time. n = 3 experiments. (**N**) MTT cell viability assay of KPPc cells after shRNA-mediated RET knockdown and in the presence of GDNF (20 ng/ml). n = 3 experiments each performed in triplicate. (**O and P**) Growth curves (O) and final weights (P) of allografted control or RET-deficient KPPc tumors, n = 10 mice each. (**Q and R**) IHC analysis of phosphorylated ERK (p-ERK) abundance in tumors from the mice in (O), n = 4. Scale bars, 200 μm. (**S**) Immunoblotting of the harvested allograft tumors in (O) for the indicated proteins. n = 3 mice from each group. (**T**) Schematic showing intratracheal administration of pSECC lentiviruses encoding Cre recombinase, CAS9, and the gRNAs sg*Tom* or sg*Ret*. (**U to W**) MRI scans (U), quantified tumor burden (V), and immunoblotting (W) at 12 and 14 weeks after delivery of the indicated Cre construct (T) in KPP mice. n = 3 mice in each group. In all panels, blots and images are representative and data are means ± SD of the stated n; $^{*}P < 0.05$ and $^{**}P < 0.01$ by unpaired Student's t test.

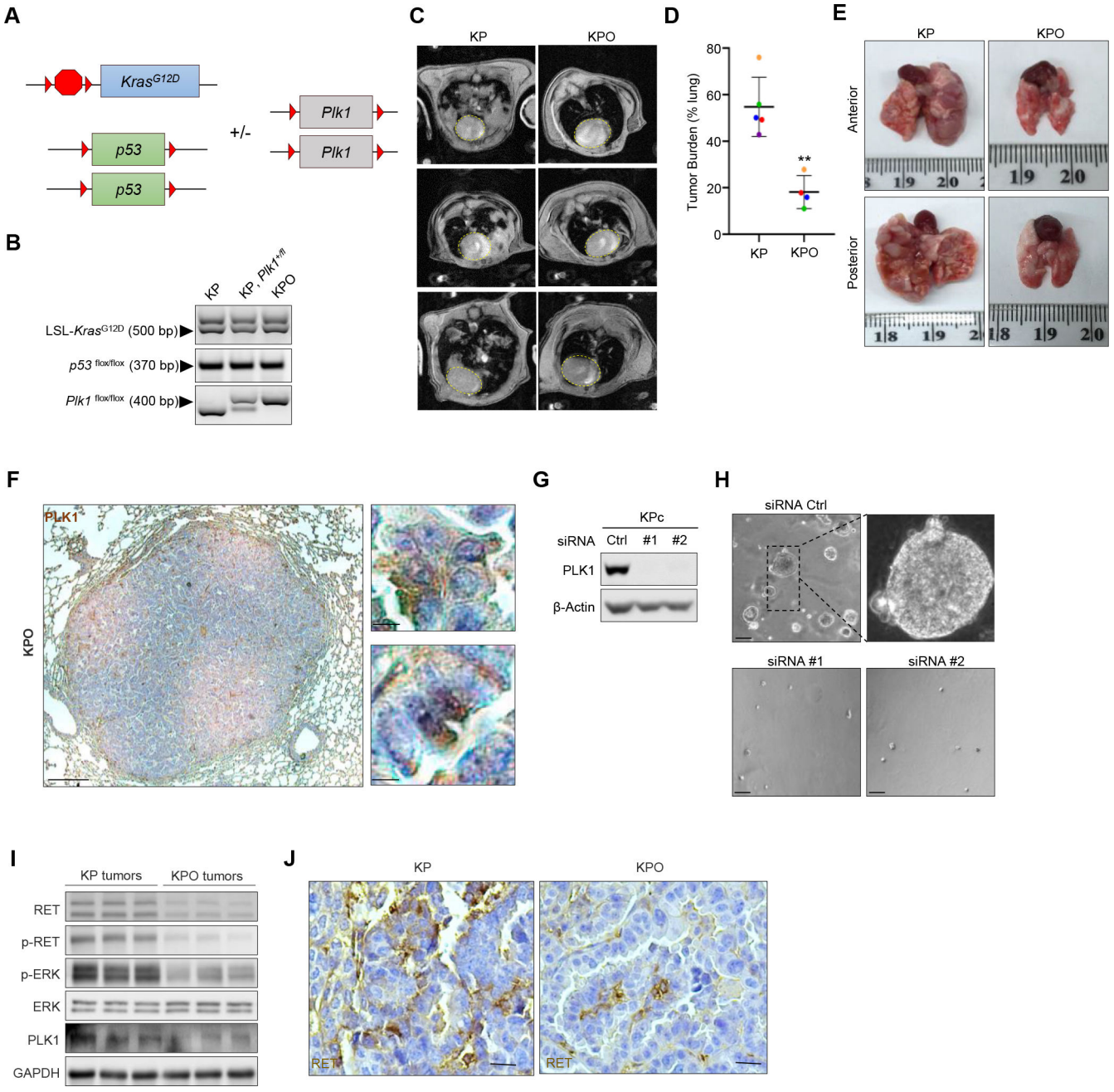

Fig.5. Elimination of PLK1 from the KP mouse model.

(**A**) Schematic of the strategy for crossing KP mice with *Plk1* knockout mice. Red triangles indicate loxP sites; red octagons indicate STOP cassettes. (**B**) Crosses confirmed by PCR using 50 ng of mouse genomic DNA. A representative of three mice each is shown. (**C** to **E**) MR imaging (C) to determine tumor burden (D) in the thorax regions of mice 12 weeks after infection with Ad-Cre; hearts are outlined by yellow circles. Representative photographs of the lungs at 14 weeks after infection are shown (E). Data are means ± SD; $n = 5$ KP and $n = 4$ KPO mice. $^{**}P < 0.01$ by unpaired Student's t test. (**F**) Representative images of IHC staining for PLK1 in a representative of the 3 observed KPO tumors. Scale bars: 200

μm and 50 μm, respectively. (**G and H**) Immunoblotting (G) and micrographs (H) of KPc cells 48 hours after transfection with each of two *Plk1*-targeted siRNAs or a control, each representative of three experiments. Scale bars: 50 μm. (**I**) Immunoblotting of single primary tumor lysates from 3 KP and 3 KPO lung tumors. (**J**) IHC staining for RET in KP and KPO tumors, representative of three each. Scale bars: 100 μm.

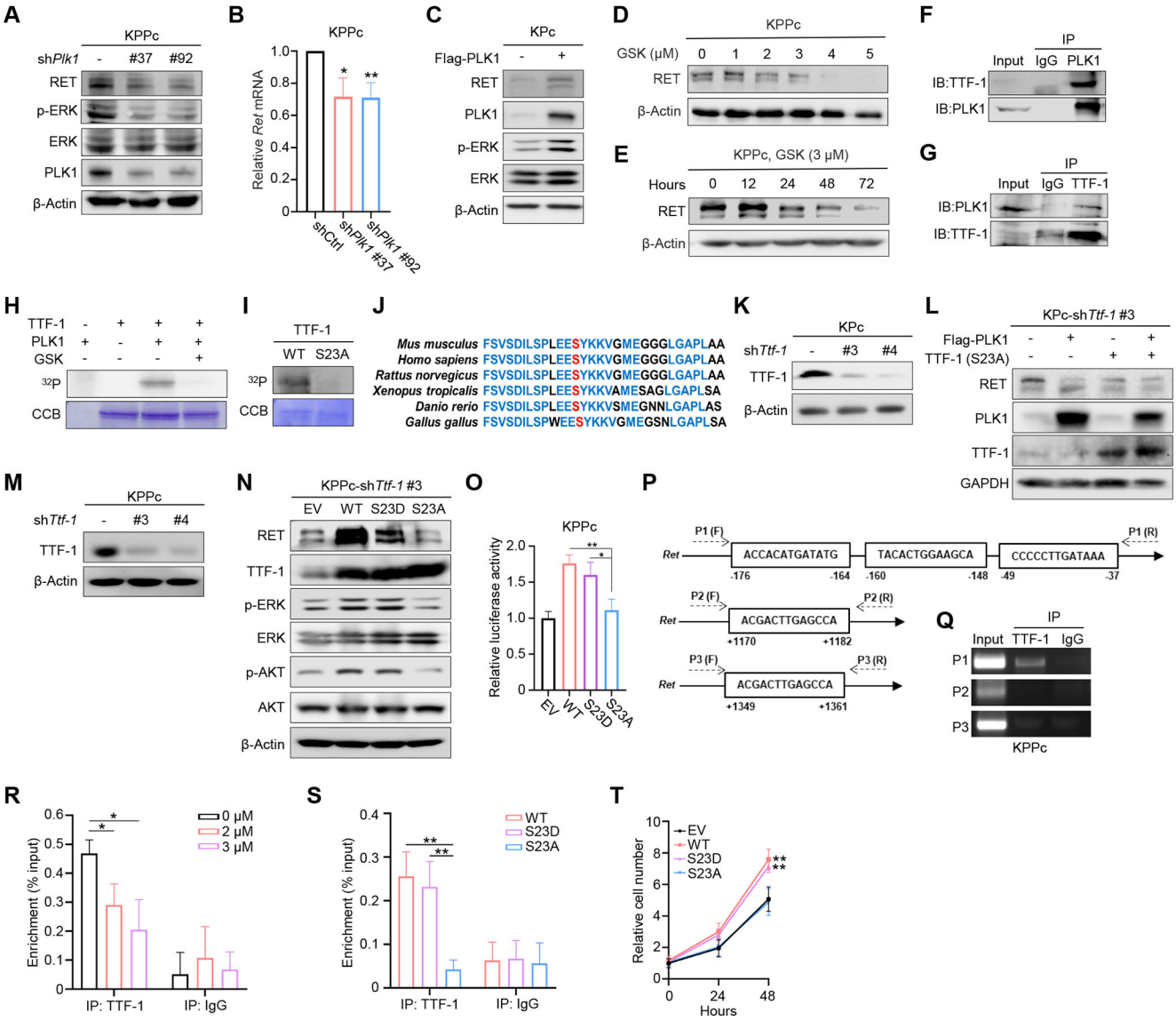

Fig.6. regulates *Ret* expression via phosphorylation of TTF-1.

(**A** and **B**) Immunoblotting (A) and qRT-PCR analysis (B) in KPPc cells stably transfected with each of two lentiviral shRNAs targeting *Plk1* (sh*Plk1* #37 and sh*Plk1* #92) or a non-target control (shCtrl). (**C**) Immunoblotting of lysates from KPc cells stably transfected with Flag-PLK1 or empty vector. (**D and E**) Immunoblotting KPPc cells were treated with GSK461364 (GSK) at the indicated concentrations for 48 hours (D) or at 3 μM and harvested at the indicated time points (E). (**F** and **G**) Immunoblotting of lysates from KPPc cells before (input) and after immunoprecipitation (IP) with antibodies against TTF-1 or PLK1 or with control IgG. (**H**) Blotting of in vitro kinase assays of recombinant TTF-1 incubated with purified PLK1 in the presence of [γ−^{32}P] ATP ± 10 nM of GSK. CCB, Coomassie brilliant blue. (**I**) In vitro kinase assays of purified PLK1 incubated with recombinant wild-type (WT) or S23A-mutant TTF-1. (**J**) Sequence context of TTF1-Ser^{23}

across various species. (**K**) Immunoblotting of KPc cells stably transfected with shRNAs targeting the TTF-1 3'-UTR (sh*Ttf-1* #3) or its coding sequence (CDS; sh*Ttf-1* #4) or a non-targeted control (shCtrl). (**L**) Immunoblotting of lysates from KPc cells transfected with Flag-PLK1 or S23A-TTF1 after endogenous TTF-1 was stably knocked down by sh*Ttf-1* #3. (**M and N**) Immunoblotting of lysates from KPPc cells stably transfected with shRNAs sh*Ttf-1* #3 or sh*Ttf-1* #4 or shCtrl (M) or with sh*Ttf-1* #3 then wild-type, S23D, or S23A TTF-1 (N). (**O**) Luciferase assay in KPPc cells co-transfected with the *Ret* promoter construct and wild-type, S23D or S23A TTF-1 for 48 hours. (**P and Q**) Schematic of the binding sequences within the *Ret* promoter relative to the designed primers, P1 to P3, used in ChIP analysis of TTF-1 binding to the *Ret* promoter region in KPPc cells. A representative of three experiments is shown. (**R and S**) ChIP followed by qPCR analysis to assess enrichment of IgG and TTF-1 at the *Ret* promoter in KPPc cells either treated with GSK461364 at the indicated concentration (R) or transfected with wild-type, S23D, or S23A TTF-1 after knockdown of endogenous TTF-1 (S). (**T**) MTT viability assay of KPPc cells transfected with empty vector (EV), wild-type TTF-1, or S23A-TTF-1. In all panels, blots are representative of three experiments, and data are means ± SD, $n = 3$ experiments; $^{*}P < 0.05$ and $^{**}P < 0.01$ by unpaired Student's *t* test.

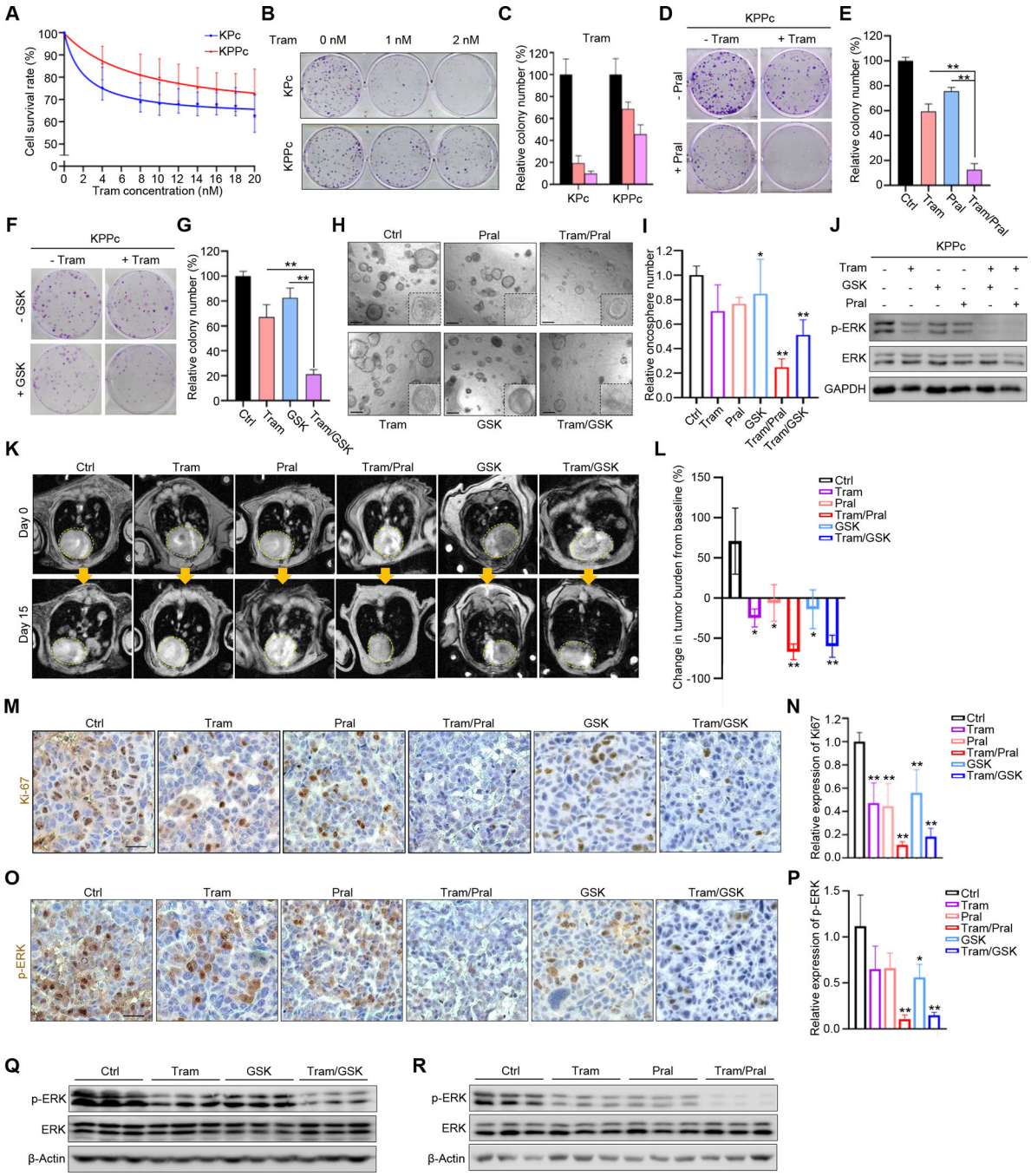

Fig.7. Efficacy of combination therapies.

(**A to C**) MTT-based viability at 48 hours (A) and clonogenic growth (B and C) of KPc and KPPc cells after treatment with trametinib (Tram) at the indicated concentrations. n = 3 experiments. (**D** and **E**) Clonogenic growth of KPPc cells treated with trametinib (Tram, 1 nM), pralsetinib (Pral, 2.5 μM; D and E) or GSK461364 (GSK, 5 nM; F and G), or the respective combination for 7 days. n = 3 experiments. (**H** and **I**) Micrographs and quantitative analysis of KPPc cell oncospheres treated with trametinib (1 nM), GSK461364 (5 nM), pralsetinib (2.5 μM), the trametinib combination for 12 days. n = 3 experiments.

(**J**) Immunoblotting of KPPc cells treated with trametinib (4 nM), GSK461364 (3 μM), pralsetinib (10 μM), or the trametinib combination for 48 hours. $n = 3$ experiments. (**K** to **R**) established lung tumors in KPP mice treated with vehicle (QD), Tram (1 mg/kg, QD), Pral (6 mg/kg, QD), Tram (1 mg/kg, QD) + Pral (6 mg/kg, QD), GSK (20 mg/kg, every 2 days) or Tram (1 mg/kg, QD) + GSK (20 mg/kg, every 2 days) for 2 weeks, MR imaging was performed (K), and the change in tumor burden was quantified (L) in mice from each group, and Ki-67 (M and N) and phosphorylated-ERK (O and P) abundance by immunohistochemistry, and others by immunoblotting (Q and R), were assessed in lung tumors from each cohort. Scale bars, 100 μm. $n = 3$ mice in each group. Data are means ± SD from n as indicated; $^{*}P < 0.05$ and $^{**}P < 0.01$ by unpaired Student's t test.